The Role of Amplitude on Controlling Flow Separation Using Traveling Wave Morphing

U. Ogunka*,A. M. Akbarzadeh †, I. Borazjani.‡
J. Mike Walker '66 Department of Mechanical engineering, Texas A&M University, College Station, TX, 77840

Large eddy simulations (LES) of a low Reynolds number flow (Re=50,000) over a NACA18 airfoil at stall angle of attack of 15 degrees are performed. The suction side of the airfoil undergoes a surface morphing in the form of backward traveling waves, simulated using our curvilinear immersed boundary method (CURVIB), to control the flow separation and enhance the aerodynamic performance. The amplitude of the morphing is in the range of $a = 0.00006L$ **to** $a = 0.004L$**,** L **: chord length, which is in the same range can be created via piezoelectric actuators. The simulations are also performed for various reduced frequencies (**$f^* = fL/U$**,** f **: frequency,** U**: free stream velocity) ranging from** $f^* = 4$ **to** 20**. The results of the simulations show that the lift coefficient,** C_L**, increases by about** 16% **and the drag coefficient,** C_D**, decreases by about** 58% **within the frequency range from** $f^* = 6$ **to** $f^* = 12$**, and the amplitude range from** $a^* = 0.001$ **to** $a^* = 0.004$**. The frequency range of the traveling wave actuation matches the range of the shedding frequency in the shear layer of the unactuated case (**$f^* = 4$ **to** $f^* = 10$**).**

I. Introduction

Flow control at low Reynolds numbers ($Re < 500,000$) is of interest for aeronautical vehicles such as micro-air vehicles (MAVs) and small unmanned aerial vehicles (UAVs). At low Reynolds numbers, the boundary layer remains laminar which may separate from the suction side of an airfoil when angle of attack (AOA) is higher than the stall angle. Boundary layer separation creates performance losses, e.g., an increase in the drag and a decrease in the lift. To reduce the effects of flow separation, boundary layer control techniques such as active and passive techniques have been adopted. Passive flow control techniques include roughness bumps, mechanical turbulators such as vortex generators, boundary layer trips, etc. Vortex generators have been observed to improve the aerodynamic performance of an airfoil

*PhD student, J. Mike Walker '66 Department of Mechanical engineering, Texas A& M University, College Station, TX
†PhD candidate, J. Mike Walker '66 Department of Mechanical engineering, Texas A& M University, College Station, TX
‡Associate Professor, J. Mike Walker '66 Department of Mechanical engineering, Texas A& M University, College Station, TX

at low Re [1, 2]. Various active flow control techniques such as steady blowing [3, 4], periodic suction and blowing [5–10], synthetic jets (zero net mass flux) [11, 12], and surface morphing [13–15] have been applied to delay stall. The surface morphing technique is found to be an energy efficient technique, using light piezoelectric actuators [16, 17]. The piezoelectric actuators, attached along the upper surface (suction side) of the airfoil, increase the fluid's kinetic energy at the near-wall by introducing periodic perturbations to trigger flow instabilities (Tollmien-Schlicting wave). This leads to the formation of Large Coherent Structures(LCS) in the boundary layer [18–20]. These perturbations can be in the form of standing wave [13, 15, 21] or traveling wave vibrations[17, 22–25].

Active flow control via surface morphing using standing waves has been investigated in several studies [20, 26–28]. Munday et al. [15, 29] reported up to 60% decrease of flow separation for a low Reynolds (Re<50,000) airfoil at prestall angles ($AOA < 9^o$). Jones et al. [13] found a delay in the onset of stall by morphing the suction side of a NACA4415 airfoil with the fibers of piezoelectric materials that produced low amplitudes standing waves. The surface vibrations reduce flow separation by introducing instability and increasing the mixing of high momentum fluid of the separated shear layer to the low momentum fluid of the reverse flow zone [6]. Recently, Akbarzadeh and Borazjani [23, 24] showed that high reduced frequency ($fL/U > 4$) traveling waves with amplitude of $0.002 < a/L < 0.008$ can suppress the stall by directly increasing the momentum of the boundary layer. They showed that traveling waves are more effective than standing waves in terms of drag reduction and decreasing of flow separation because traveling waves can enhance the fluid momentum directly. Nevertheless, the range of amplitude of experimental traveling waves that currently can be created by piezo-electric actuators is 10^{-3}<$a/L < 6 \times 10^{-5}$ [22] that is smaller than the study of Akbarzadeh and Borazjani [23]. Therefore, the range of amplitudes at which the waves can suppress the stall needs to be obtained precisely. Moreover, in the previous study, the maximum frequency tested was $fL/U = 8.0$, and effectiveness of higher frequencies was not investigated. To find the optimum range of amplitudes and frequencies of traveling waves for flow control, several numerical simulations of a NACA18 airfoil at stall condition ($AOA = 15$) with a wavy low-amplitude traveling wave morphing are performed. Here, we test $20.0 > fL/U > 4.0$ and $10^{-3} > a/L > 6 \times 10^{-5}$ which can be created by the piezo-electric actuators [22].

In this paper, to quantify the role of amplitude and frequency on controlling flow separation using traveling wave morphing, we compute and compare the aerodynamics of an unactuated NACA18 airfoil case and backward traveling wave actuated NACA18 airfoil cases with different frequencies and amplitudes. The governing equations, computational

mesh and the numerical methods are described in Section II. The lift and drag coefficient of the NACA18 airfoil for different frequencies and amplitudes are compared against an unactuated NACA18 airfoil (Section III). The observed trends are explained by visualizing the flow field using the vorticity (Section III). Finally, the results are discussed and the conclusions are reported in Section IV.

II. Method

Numerical simulations are performed for a NACA18 airfoil near the stall angle of attack ($AOA = 15^o$) at which the flow starts to separate from the leading edge, and a large reverse flow is generated on the suction side of the airfoil. The structure of the simulation and the numerical method employed for solving the problem are similar to our previous publications [23, 24]. The free stream velocity (U) and the airfoil chord length (L) are, respectively, the characteristic velocity and length, and $Re = UL/\nu = 50,000$, where ν is the kinematic viscosity. The suction side of the airfoil undergoes a backward traveling wave deformation as shown in Fig. 1a. To calculate the new position of the suction side of the airfoil under motion in the original Cartesian frame (x, y, z), a local frame (X, Y, Z) is defined, i.e. its origin is at the leading edge and is rotated by the angle of attack (Fig. 1b). The backward traveling wave oscillation ($h(X,t)$) prescribed along Y direction, is:

$$h^*(X,t) = a^*(X)\sin(2\pi(f^*t^* - X^*/\lambda^*)), \tag{1}$$

where $h^* = h/L$ is the non-dimensional displacement of the suction-side, $f^* = fL/U$ is the reduced frequency, $\lambda^* = \lambda/L$ is the non-dimensional wavelength, and $t^* = tU/L$ is the non-dimensional time, $X^* = X/L$ is the non-dimensional streamwise length that starts from the leading edge, and $a^*(X) = a(X)/L$ is the amplitude of the wave which starts from $X = 0.1L$ to $X = 0.85L$. The amplitude is constant and equal to its maximum value a^*_{max} from $X = 0.2L$ to $X = 0.8L$ and decreases linearly toward the leading and trailing edges. Here, the parameters with (*) symbol are nondimensional.

The governing equations for the flow are the unsteady, three-dimensional, incompressible, filtered Navier-Stokes and continuity equations. The governing Eqns. are discretized via a second order central scheme and integrated in time using a second-order fractional-step methodology. The momentum equations are solved with a Newton-Krylov method with an approximate analytical Jacobian solver [30], and the pressure Poisson equation is solved using GMRES solver with a multigrid preconditioner [31].

The turbulent flow is modeled with a large eddy simulation (LES) method. Here, a dynamic subgrid-scale model

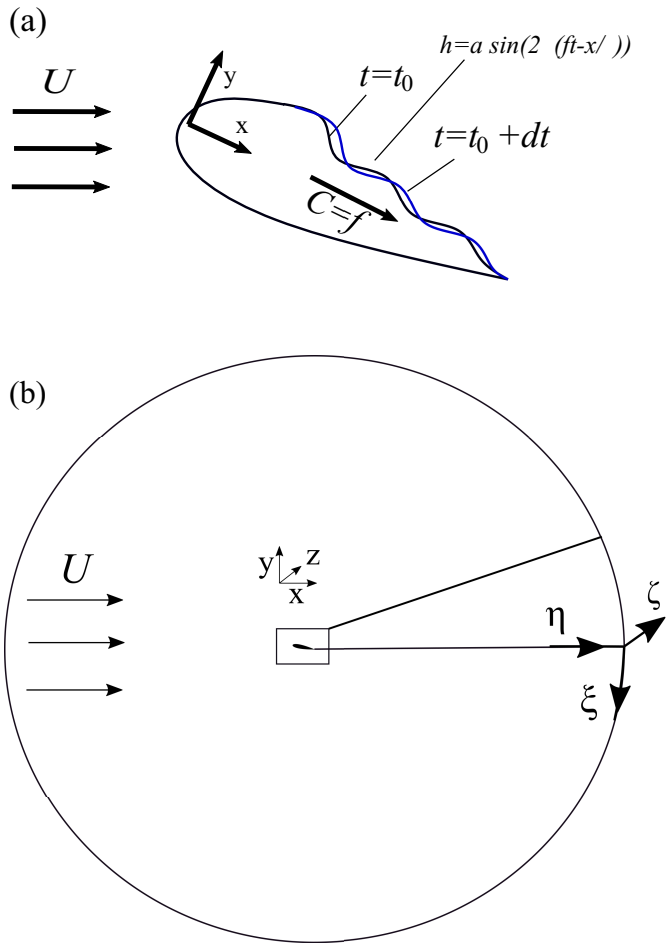

Fig. 1 (a) The schematic of traveling wave surface morphing and (b) the simulation setup with an O-grid mesh

[32] is used to compute the subgrid stress tensor since previous studies [33, 34] have shown that subgrid-scale models are suitable for modeling transitional turbulent flows. The LES is validated for modeling transitional and turbulent flows, e.g., inclined plates [35] and circular cylinders [36], and has been used in different applications such as aquatic swimming [36] and vortex flow [37]. The detail of our LES modeling can be found in previous studies [38, 39].

The computational mesh is same as previous study [23], as presented in Fig.1b. The grid adopted for the fluid domain is an O-grid generated in curvilinear coordinates (ξ, η, ζ) where η is normal to the airfoil surface, and ξ is parallel to the airfoil surface. The grid is extruded in the ζ direction for $0.1L$ to generate a 3D domain. The boundary conditions along ξ and ζ is periodic. On the outer boundary η, the upstream is characterized by an inlet velocity ($u_x = U$) at $x < 0$, while the downstream is characterized with a Neumann boundary condition with a mass flux correction at $x > 0$. The grid resolution is maintained at $0.0003L$ along η direction near the airfoil surface that corresponds to a wall unit spacing of $\eta^+ = 0.9$. The grid spacing is constant until $\eta = 0.022$, then it increases with a hyperbolic function to the boundaries.

The time step is $0.001L/U$ for the baseline case and it ranges from $0.00021L/U$ to $0.00048L/U$ for the actuated cases. More details on the simulation set-up, grid sensitivity study, and validation can be found in our previous studies [23, 24].

The moving boundaries are handled using the sharp interface immersed boundary (IB) method, which is explained in the previous publications [31, 40]. In this method, the background mesh is fixed and the velocities of the fluid points adjacent to the moving boundaries (immersed nodes) are computed using an interpolation along the surface normal. The classification of domain into solid, immersed, and fluid nodes is performed by a ray tracing algorithm [41]. The ray tracing algorithm method is validated for flows with moving boundaries [41] and has been applied in simulations involving biological flows [37, 42, 43].

To quantify the aerodynamic performance of the NACA18 airfoil, the mean lift coefficient $\overline{C}_L = \overline{F}_L/0.5\rho U^2 L$, mean drag coefficient $\overline{C}_D = \overline{F}_D/0.5\rho U^2 L$ and standard deviation (σ) are computed by averaging the final 40,000 number of iterations for 10 cycles for the cases reported in table 1. $\overline{F}_L$ is the mean force per unit airfoil span acting along the y direction, $\overline{F}_D$ is the mean force per unit airfoil span acting along the x direction, and ρ is the fluid density. The statistical student t-test was employed to compare the mean C_L and C_D of the NACA18 airfoil cases. The statistical student t-test determines if the mean of two datasets are significantly different to each other ($p < 0.05$) or the means of two datasets are statistically similar ($p > 0.05$).

III. Results

Previous studies on flow control with surface morphing and traveling waves have reported that both the velocity of the actuated surface and frequency of the actuations are the main parameters that control the flow separation [23, 35]. For a traveling wave oscillation, the surface velocity increases by increasing the amplitude as it scales with f^*a^*. It also increases linearly by reduced frequency (f^*). It has been observed from the previous study [23] that the traveling waves could reattach the flow for this airfoil at the same AOA when the reduced frequency (f^*) of the wave is greater than 4, while the upper limit for the traveling wave is not known. Moreover, the range of effective amplitudes needs to be understood. Therefore, several simulations are performed to obtain the optimum amplitude and frequency that can effectively control the flow separation. The case studies are presented in Table 1. The wavelength is kept constant at $\lambda^* = 0.44$, the same as the experimental study of Olivett et al. [22]. The first case is an unactuated airfoil (baseline) and cases $2-11$ are actuated airfoils with backward traveling waves with amplitude range of $a^* = 0.00006$ to $a^* = 0.004$, and frequency range of $f^* = 4$ to $f^* = 20$. Cases 2 to 4 have the lowest amplitude ($a^* = 0.00006$) and the rest of the

cases have a significantly higher amplitudes, e.g., $a^* \geq 0.0005$. Moreover, the standard deviation is reported in table 1 to investigate the significance of the variation of the mean forces with respect to the baseline.

Table 1 The case studies, including unactuated airfoil and backward traveling wave actuation with different frequencies. $\overline{C_L}$ and $\overline{C_D}$ are lift and drag coefficients, respectively. σ_{C_L} and σ_{C_D} are the standard deviation of lift and drag coefficient. Here, case 10^* is from previous work [23].

case	f^*	a^*	$\overline{C_L}$	$\overline{C_D}$	$\sigma(C_L)$	$\sigma(C_D)$
1	0	0	0.676	0.279	0.191	0.047
2	4.0	0.00006	0.70	0.261		
3	10.0	0.00006	0.72	0.254		
4	20.0	0.00006	0.72	0.243		
5	8.0	0.0005	0.76	0.253	0.160	0.038
6	4.0	0.001	0.69	0.262	0.185	0.055
7	8.0	0.001	0.89	0.090	0.151	0.035
8	12.0	0.001	0.87	0.098	0.293	0.071
9	16.0	0.001	0.67	0.247	0.506	0.127
10^*	8.0	0.002	0.92	0.090	0.170	0.040
11	8.0	0.004	0.79	0.115	0.503	0.012

The results presented in table 1 show that a low amplitude ($a^* = 0.00006$) oscillation can only increase the lift coefficient by about 5% and decrease the drag by about 9% for high frequency actuation ($f^* = 20$) compared to the unactuated airfoil. Further increasing the amplitude (case 10^*), C_L increases by about 36% and C_D decreases by about 67%. This shows that this low amplitude oscillations ($a^* = O(10^{-5})$), cases 2 to 4, are not effective for flow control compared to the high amplitude one (case 10^*) probably because the velocity of the actuated surface due to oscillations is small $O(0.005U)$. Increasing the amplitude to $a^* = 0.0005$ for frequency actuation ($f^* = 8$), the lift increases by 12% and the drag decreases by 9% compared to the unactuated case. A further increase of the amplitude to $a^* = 0.001$ and keeping the frequency constant at $f^* = 8$, the lift significantly increases by 32% ($p < 0.05$) and the drag significantly decreases by 68% ($p < 0.05$). Increasing the frequency to $f^* = 12$ in case 8, the lift coefficient is statistically similar to that of case 7 ($p > 0.05$), significantly increases by 28% compared to the unactuated case ($p < 0.05$). However, the drag is significantly different from case 7 ($p < 0.05$) and has significantly decreased by 65% compared to the unactuated case. Compared to case 10^*, cases $7 - 8$ show that an amplitude of $a^* = 0.001$ and frequency of $f^* = 8$ to $f^* = 12$ are effective for flow control. Increasing the amplitude or frequency beyond this point causes a significant lift decrease below 23% ($p < 0.05$) and a significant drag increase above 28% ($p < 0.05$) compared to the unactuated case.

The effect of amplitude on the mean C_L and C_D is presented in Figs. 2 and 3, respectively. Figure 2 shows that the

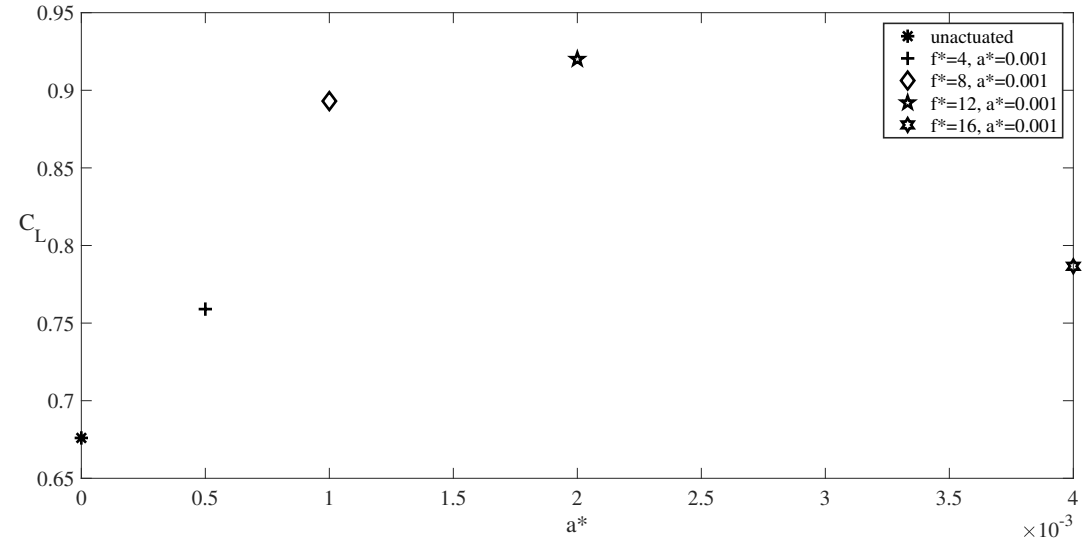

Fig. 2 Effect of amplitude of the traveling wave on the lift coefficient (C_L) for airfoil at AOA = 15^0 with frequency $f^* = 8$.

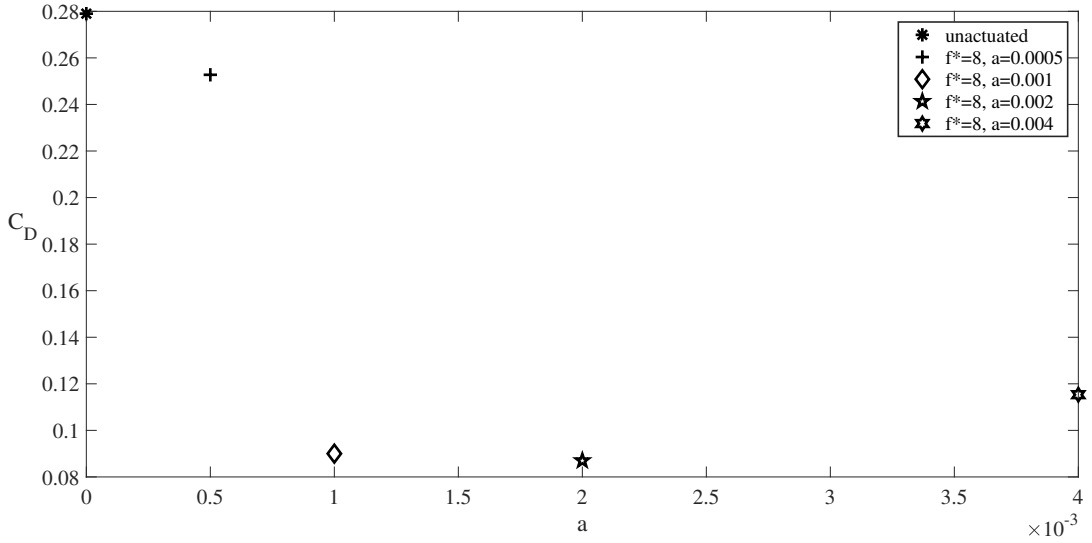

Fig. 3 Effect of amplitude of the traveling wave on the drag coefficient (C_D) for airfoil at AOA = 15^0 with frequency $f^* = 8$.

C_L significantly increases ($p < 0.05$) with increase in the amplitude to $a^* = 0.002$. By increasing the amplitude to $a^* = 0.004$, C_L significantly decreases ($p < 0.05$) compared to $a^* = 0.002$. At $a^* = 0.0005$, the lift increases by 12% compared to the unactuated case. Increasing the amplitude to $a^* = 0.001$, the lift significantly increases by 32% ($p < 0.05$) compared to the unactuated case. A further increase in the amplitude to $a^* = 0.002$ sees the lift significantly increase by 36% ($p < 0.05$) compared to the unactuated flow case. Increasing the amplitude to $a^* = 0.004$, the lift

significantly decreases by 18% ($p < 0.05$) compared to the $a^* = 0.002$ case, and significantly increases by 16% ($p < 0.05$) compared to the unactuated case.

As shown in Fig.3 it can be observed that the C_D significantly decreases ($p < 0.05$) with an increase in the amplitude to $a^* = 0.002$. Increasing the amplitude to $a^* = 0.004$ leads to a significant increase ($p < 0.05$) in C_D compared to $a^* = 0.002$. At $a^* = 0.0005$, the drag reduces by 9% compared to the unactuated case. Increasing the amplitude to $a^* = 0.001$, the drag significantly decreases by 68% ($p < 0.05$) compared to the unactuated case. A further increase in the amplitude to $a^* = 0.002$, the drag significantly reduces by 68% ($p < 0.05$) compared to the unactuated flow case. Increasing the amplitude to $a^* = 0.004$, the drag significantly increases by approximately 33% ($p < 0.05$) compared to the $a^* = 0.002$ case, and significantly reduces by 58% ($p < 0.05$) compared to the unactuated case.

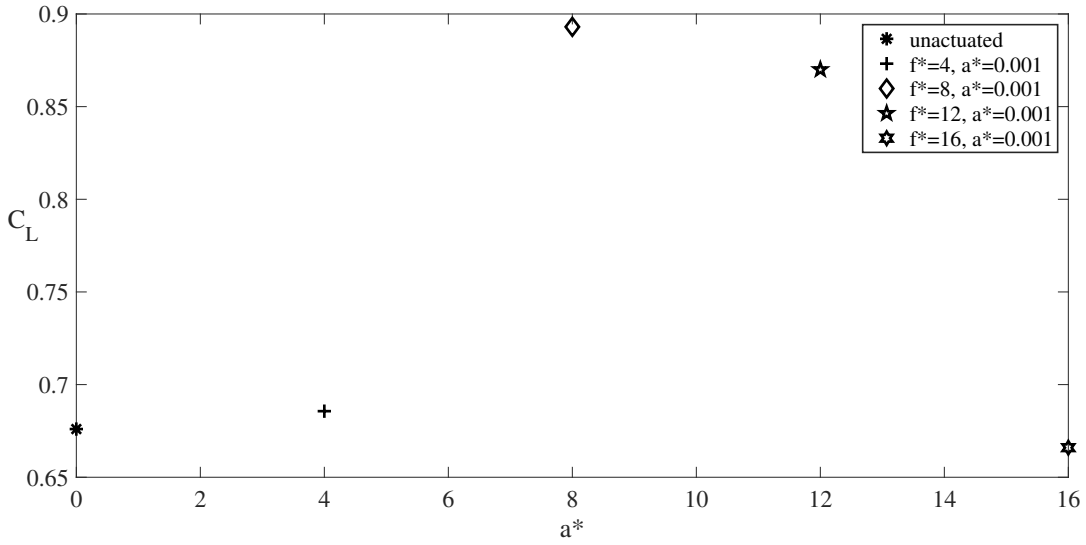

Fig. 4 Effect of frequency of the traveling wave on the lift coefficient (C_L) for airfoil at AOA = 15^0 with frequency $a^* = 0.001$.

The effect of frequency on the mean C_L and C_D is presented in Figs. 4 and 5, respectively. It can be observed that C_L significantly increases ($p < 0.05$) when the frequency increases to $f^* = 8$ in case 7. Increasing the frequency to $f^* = 12$ in case 8, the C_L decreases but is statistically similar to case 7 ($p > 0.05$). However, by increasing the frequency $f^* = 16$, the C_L significantly decreases ($p < 0.05$) compared to $f^* = 8$ and $f^* = 12$. At $f^* = 4$, the lift increases by 1.4% compared to the unactuated case. Increasing the frequency to $f^* = 8$, the lift significantly increases by 32% ($p < 0.05$) compared to the unactuated case. A further increase in the frequency to $f^* = 12$, the lift decreases by 2.6% compared to the $f^* = 8$ case, and significantly increases by 29% ($p < 0.05$) compared to the unactuated case.

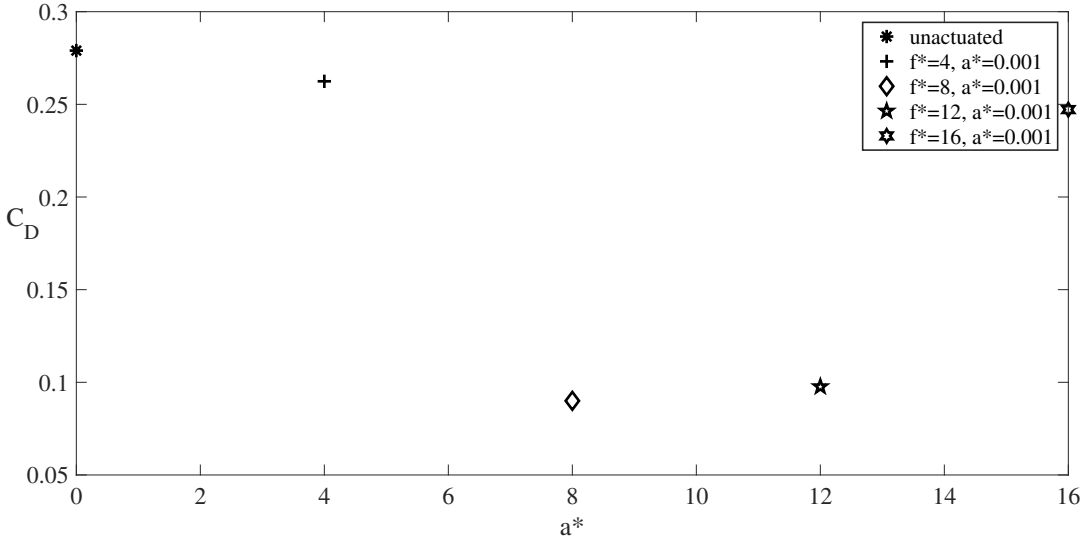

Fig. 5 Effect of frequency of the traveling wave on the drag coefficient (C_D) for airfoil at AOA = 15^0 with frequency $a^* = 0.001$.

Surprisingly, by increasing the frequency to $f^* = 16$, the lift significantly ($p < 0.05$) decreases by 23% compared to the $f^* = 12$ case, and decreases by 1.5% compared to the unactuated case.

The plot of C_D indicates the C_D significantly decreases ($p < 0.05$) with an increase in the frequency to $f^* = 8$. Increasing the frequency to $f^* = 12$ and $f^* = 16$, the C_D significantly increases ($p < 0.05$) compared to $f^* = 8$. At $f^* = 4$, the drag reduces by 6% compared to the unactuated case. Increasing the frequency to $f^* = 8$, the drag significantly reduces ($p < 0.05$) by 68% compared to the unactuated case. A further increase in the frequency to $f^* = 12$, the drag significantly increases ($p < 0.05$) by 8.5% compared to the $f^* = 8$ case, and significantly reduces ($p < 0.05$) by 65% compared to the unactuated flow case. Increasing the frequency to $f^* = 16$, the drag significantly increases ($p < 0.05$) by approximately 153% compared to the $f^* = 12$ case, and reduces by 11% compared to the unactuated case.

The effect of oscillations for all the cases can be observed by instantaneous contours of out-of-plane vorticity in Fig. 6 at five different times. For cases 1 to 4, the flow is highly separated, i.e., the shear layer separates from the leading edge of the airfoil and a large recirculatory zone, i.e., trailing edge vortex, is generated near the trailing edge. Note that flow visualization for case 3 (Fig. 6b1-b5) represents the low amplitude cases 2, 3, and 4, as the flow was not affected by changing the frequency at the low amplitude cases. Further increase of the amplitude to $a^* = 0.0005$, also, did not suppress the flow separation, as a large trailing edge vortex can be observed in Fig.6e5. However, by increasing the amplitude of the oscillation in case to $a^* = 0.001$ and keeping the frequency in the range of 8 to 12

(Fig.6), the shear layer is attached on the leading edge of the airfoil. Nevertheless, by increasing the frequency in case 9 to $f^* = 16$ or decreasing the frequency in case 6 to $f^* = 4$, the shear layer separation and trailing edge vortex increases. The formation and shedding the trailing edge vortex results in the lift oscillation and stall of the airfoil. The flow visualizations, similar to the plots of C_L and C_D suggest that the optimal range of frequency and amplitude for suppressing the stall are $8 \leq f^* \leq 12$ and $0.001 \leq a^* \leq 0.002$, respectively.

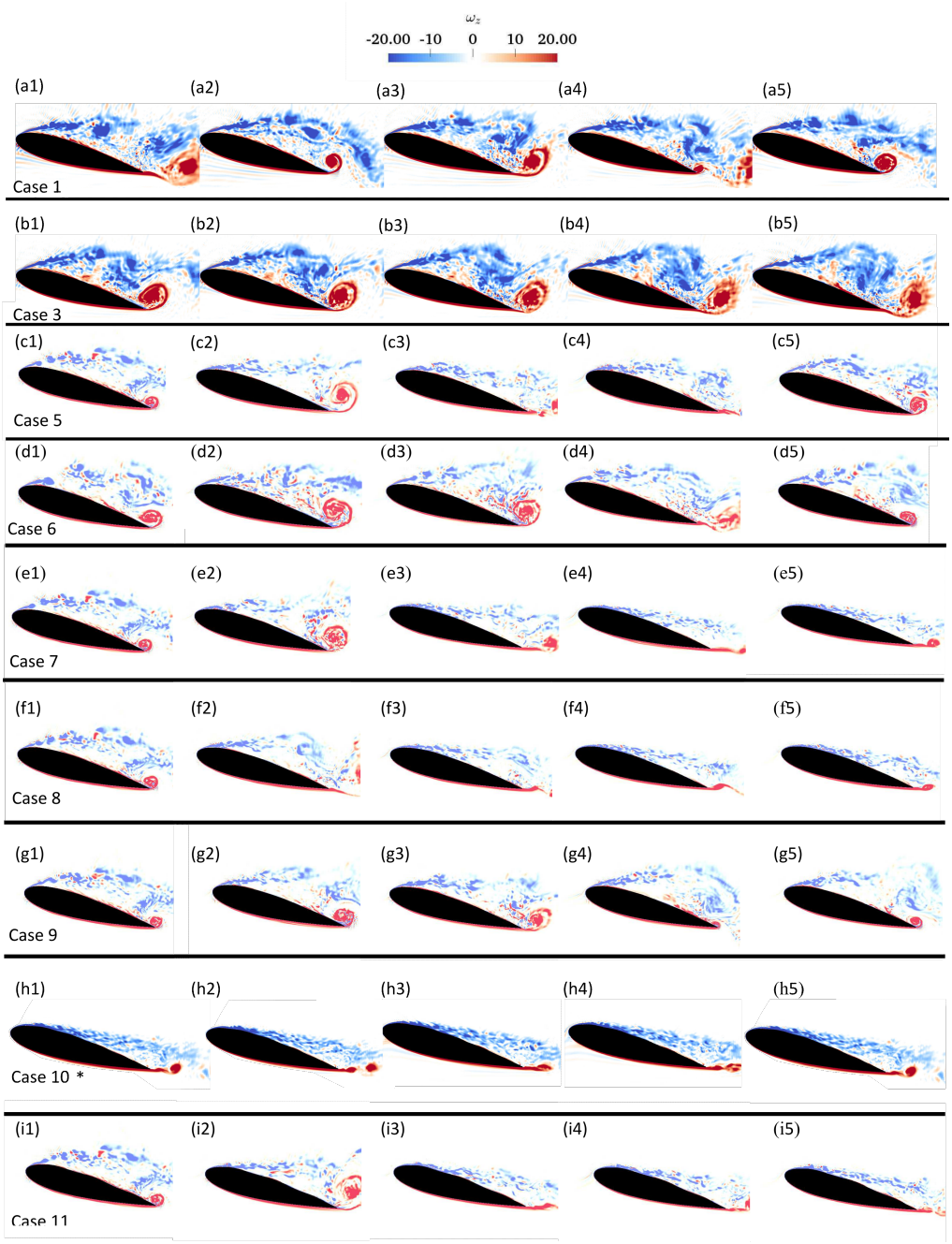

Fig. 6 The contour of instantaneous vorticity for a backward traveling wave actuated airfoil.

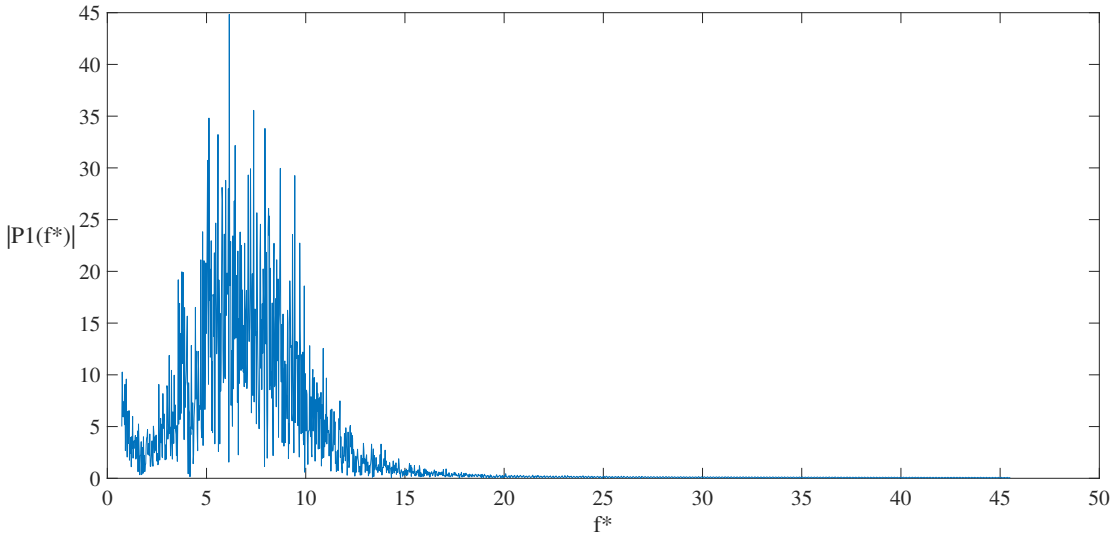

Fig. 7 The FFT plot of the power spectrum of the velocity (P_1) vs. the frequency domain for unactuated airfoil at AOA = 15^0 at the leading edge.

To identify the correlation between the optimum excitation frequency and the shedding frequency, the vortex shedding frequency that occurs at the leading edge of the NACA18 airfoil is investigated. Fig. 7 shows the power spectrum of the frequency domain for the unactuated airfoil. The spectrum is computed by spectrum analysis of u_x at a point near the leading edge, i.e., at $x = 0.0833L$ and $y = 0.273L$ with respect to the origin (Fig. 1b). The plot indicates the shedding frequency of the shear layer is in the range of $f^* = 4$ to $f^* = 10$. This is similar to the range of frequency where the maximum lift enhancement and drag reduction was observed. This suggests that backward traveling wave oscillations with a frequency, f^*, range equal to or closely equal to the vortex shedding frequency range can suppress the stall and improve the aerodynamic performance of the airfoil.

IV. Conclusions and the future work

Effect of low amplitude traveling waves with various reduced frequencies and amplitudes ranging from $f^* = 4$ to $f^* = 20$, and amplitudes ranging from $a^* = 0.00006$ to $a^* = 0.004$, respectively, are investigated on flow separation and aerodynamic performance of a NACA18 airfoil at stall condition ($AOA = 15^o$). The flow visualizations, and plots of C_D and C_L suggest that the range of frequency and amplitude for maximum lift enhancement and drag reduction are $8 \leq f^* \leq 12$ and $0.001 \leq a^* \leq 0.004$, respectively. Within these frequency and amplitude ranges, the lift increases above 16%, the drag decreases more than 58% compared to the unactuated case and the stall is suppressed. Outside

this range, the coefficient of lift, C_L, increases below 13% and the coefficient of drag, C_D, decreases less than 12% compared to the unactuated case. The frequency range of the traveling wave actuation matches the range of the shedding frequency in the shear layer of the unactuated case ($f^* = 4$ to $f^* = 10$).

Acknowledgments

This work was partly supported by the National Science Foundation (NSF) career grant CBET 1453982 and 1905355. The computational resources were partly provided by the High Performance Research Computing (HPRC) facilities at Texas A&M University.

References

[1] Lin, J. C., "Review of research on low-profile vortex generators to control boundary-layer separation," *Progress in Aerospace Sciences*, Vol. 38, No. 4-5, 2002, pp. 389–420.

[2] Manolesos, M., and Voutsinas, S. G., "Experimental investigation of the flow past passive vortex generators on an airfoil experiencing three-dimensional separation," *Journal of Wind Engineering and Industrial Aerodynamics*, Vol. 142, 2015, pp. 130–148.

[3] Aubrun, S., McNally, J., Alvi, F., and Kourta, A., "Separation flow control on a generic ground vehicle using steady microjet arrays," *Experiments in Fluids*, Vol. 51, No. 5, 2011, pp. 1177–1187. https://doi.org/10.1007/s00348-011-1132-0.

[4] Donovan, J., Kral, L., and Cary, A., "Active flow control applied to an airfoil," *36th AIAA Aerospace Sciences Meeting and Exhibit*, American Institute of Aeronautics and Astronautics, 1998. https://doi.org/10.2514/6.1998-210.

[5] Greenblatt, D., and Wygnanski, I. J., "The control of flow separation by periodic excitation," *Progress in aerospace Sciences*, Vol. 36, No. 7, 2000, pp. 487–545.

[6] Seifert, A., Darabi, A., and Wyganski, I., "Delay of airfoil stall by periodic excitation," *Journal of Aircraft*, Vol. 33, No. 4, 1996, pp. 691–698. https://doi.org/10.2514/3.47003.

[7] WU, J.-Z., LU, X.-Y., DENNY, A. G., FAN, M., and WU, J.-M., "Post-stall flow control on an airfoil by local unsteady forcing," *Journal of Fluid Mechanics*, Vol. 371, 1998, pp. 21–58. https://doi.org/10.1017/s0022112098002055.

[8] Glezer, A., and Amitay, M., "Synthetic jets," *Annual review of fluid mechanics*, Vol. 34, No. 1, 2002, pp. 503–529.

[9] Amitay, M., Smith, D. R., Kibens, V., Parekh, D. E., and Glezer, A., "Aerodynamic Flow Control over an Unconventional Airfoil Using Synthetic Jet Actuators," *AIAA Journal*, Vol. 39, No. 3, 2001, pp. 361–370. https://doi.org/10.2514/2.1323.

[10] Buchmann, N. A., Atkinson, C., and Soria, J., "Influence of ZNMF jet flow control on the spatio-temporal flow structure over a NACA-0015 airfoil," *Experiments in Fluids*, Vol. 54, No. 3, 2013. https://doi.org/10.1007/s00348-013-1485-7.

[11] Rodríguez Pérez, I. M., Lehmkuhl, O., and Borrell Pol, R., "Effects of the actuation on the boundary layer of an airfoil at Reynolds Number Re= 60000," *Flow turbulence and combustion*, 2020, pp. 1–20.

[12] Glezer, A., "Some aspects of aerodynamic flow control using synthetic-jet actuation," *Philosophical Transactions of the Royal Society A: Mathematical, Physical and Engineering Sciences*, Vol. 369, No. 1940, 2011, pp. 1476–1494.

[13] Jones, G., Santer, M., Debiasi, M., and Papadakis, G., "Control of flow separation around an airfoil at low Reynolds numbers using periodic surface morphing," *Journal of Fluids and Structures*, Vol. 76, 2018, pp. 536–557.

[14] Park, Y. W., Lee, S.-G., Lee, D.-H., and Hong, S., "Stall Control with Local Surface Buzzing on a NACA 0012 Airfoil," *AIAA Journal*, Vol. 39, No. 7, 2001, pp. 1400–1402. https://doi.org/10.2514/2.1460.

[15] Munday, D., and Jacob, J., "Active Control of Separation on a Wing with Oscillating Camber," *Journal of Aircraft*, Vol. 39, No. 1, 2002, pp. 187–189. https://doi.org/10.2514/2.2915.

[16] Seifert, A., Eliahu, S., Greenblatt, D., and Wygnanski, I., "Use of Piezoelectric Actuators for Airfoil Separation Control," *AIAA Journal*, Vol. 36, No. 8, 1998, pp. 1535–1537. https://doi.org/10.2514/2.549.

[17] Musgrave, P. F., and Tarazaga, P. A., "Turbulent Boundary Layer over a Piezoelectrically Excited Traveling Wave Surface," *AIAA Scitech 2019 Forum*, 2019, p. 1354.

[18] Greenblatt, D., and Wygnanski, I. J., "The control of flow separation by periodic excitation," *Progress in aerospace Sciences*, Vol. 36, No. 7, 2000, pp. 487–545.

[19] Seifert, A., Darabi, A., and Wyganski, I., "Delay of airfoil stall by periodic excitation," *Journal of aircraft*, Vol. 33, No. 4, 1996, pp. 691–698.

[20] Jones, G., Santer, M., and Papadakis, G., "Control of low Reynolds number flow around an airfoil using periodic surface morphing: A numerical study," *Journal of Fluids and Structures*, Vol. 76, 2018, pp. 95–115.

[21] Jones, G., Santer, M., and Papadakis, G., "Control of low Reynolds number flow around an airfoil using periodic surface morphing: A numerical study," *Journal of Fluids and Structures*, Vol. 76, 2018, pp. 95–115. https://doi.org/10.1016/j.jfluidstructs.2017.09.009.

[22] Olivett, A., Corrao, P., and Karami, M., "Flow Control and Separation Delay in Morphing Wing Aircraft Using Traveling Wave Actuation," *ASME 2020 Conference on Smart Materials, Adaptive Structures and Intelligent Systems*, American Society of Mechanical Engineers Digital Collection, 2020.

[23] Akbarzadeh, A., and Borazjani, I., "Controlling Flow Separation on a Thick Airfoil Using Backward Traveling Waves," *AIAA Journal*, 2020, pp. 1–8.

[24] Akbarzadeh, A., and Borazjani, I., "A numerical study on controlling flow separation via surface morphing in the form of backward traveling waves," *AIAA Aviation 2019 Forum*, 2019, p. 3589.

[25] Albers, M., Meysonnat, P. S., and Schröder, W., "Actively reduced airfoil drag by transversal surface waves," *Flow, Turbulence and Combustion*, Vol. 102, No. 4, 2019, pp. 865–886.

[26] Kang, W., Lei, P., Zhang, J., and Xu, M., "Effects of local oscillation of airfoil surface on lift enhancement at low Reynolds number," *Journal of Fluids and Structures*, Vol. 57, 2015, pp. 49–65.

[27] Munday, D., and Jacob, J., "Active control of separation on a wing with oscillating camber," *Journal of aircraft*, Vol. 39, No. 1, 2002, pp. 187–189.

[28] Di, G., Wu, Z., and Huang, D., "The research on active flow control method with vibration diaphragm on a NACA0012 airfoil at different stalled angles of attack," *Aerospace Science and Technology*, Vol. 69, 2017, pp. 76–86.

[29] Munday, D., Jacob, J., Hauser, T., and Huang, G., "Experimental and Numerical Investigation ofAerodynamic Flow Control Using Oscillating Adaptive Surfaces," *1st Flow Control Conference*, American Institute of Aeronautics and Astronautics, 2002. https://doi.org/10.2514/6.2002-2837.

[30] Asgharzadeh, H., and Borazjani, I., "A Newton–Krylov method with an approximate analytical Jacobian for implicit solution of Navier–Stokes equations on staggered overset-curvilinear grids with immersed boundaries," *Journal of computational physics*, Vol. 331, 2017, pp. 227–256.

[31] Ge, L., and Sotiropoulos, F., "A numerical method for solving the 3D unsteady incompressible Navier–Stokes equations in curvilinear domains with complex immersed boundaries," *Journal of computational physics*, Vol. 225, No. 2, 2007, pp. 1782–1809.

[32] Germano, M., Piomelli, U., Moin, P., and Cabot, W. H., "A dynamic subgrid-scale eddy viscosity model," *Physics of Fluids A: Fluid Dynamics*, Vol. 3, No. 7, 1991, pp. 1760–1765.

[33] Rizzetta, D. P., Visbal, M. R., and Morgan, P. E., "A high-order compact finite-difference scheme for large-eddy simulation of active flow control," *Progress in Aerospace Sciences*, Vol. 44, No. 6, 2008, pp. 397–426.

[34] Akhavan-Safaei, A., Seyedi, S. H., and Zayernouri, M., "Anomalous features in internal cylinder flow instabilities subject to uncertain rotational effects," *Physics of Fluids*, Vol. 32, No. 9, 2020, p. 094107.

[35] Akbarzadeh, A., and Borazjani, I., "Reducing flow separation of an inclined plate via travelling waves," *Journal of Fluid Mechanics*, Vol. 880, 2019, pp. 831–863.

[36] Bottom II, R., Borazjani, I., Blevins, E., and Lauder, G., "Hydrodynamics of swimming in stingrays: numerical simulations and the role of the leading-edge vortex," *Journal of Fluid Mechanics*, Vol. 788, 2016, pp. 407–443.

[37] Asadi, H., Asgharzadeh, H., and Borazjani, I., "On the scaling of propagation of periodically generated vortex rings," *Journal of Fluid Mechanics*, Vol. 853, 2018, pp. 150–170. https://doi.org/10.1017/jfm.2018.529.

[38] Akbarzadeh, A. M., and Borazjani, I., "Large eddy simulations of a turbulent channel flow with a deforming wall undergoing high steepness traveling waves," *Physics of Fluids*, Vol. 31, No. 12, 2019, p. 125107. https://doi.org/10.1063/1.5131268.

[39] Borazjani, I., and Akbarzadeh, A., "Large Eddy Simulations of Flows with Moving Boundaries," *Modeling and Simulation of Turbulent Mixing and Reaction*, Springer, 2020, pp. 201–225.

[40] Borazjani, I., Ge, L., and Sotiropoulos, F., "Curvilinear immersed boundary method for simulating fluid structure interaction with complex 3D rigid bodies," *Journal of Computational physics*, Vol. 227, No. 16, 2008, pp. 7587–7620.

[41] Borazjani, I., Ge, L., and Sotiropoulos, F., "Curvilinear immersed boundary method for simulating fluid structure interaction with complex 3D rigid bodies," *Journal of Computational physics*, Vol. 227, No. 16, 2008, pp. 7587–7620.

[42] Ogunka, U. E., Daghooghi, M., Akbarzadeh, A. M., and Borazjani, I., "The Ground Effect in Anguilliform Swimming," *Biomimetics*, Vol. 5, No. 1, 2020, p. 9.

[43] Asgharzadeh, H., Asadi, H., Meng, H., and Borazjani, I., "A non-dimensional parameter for classification of the flow in intracranial aneurysms. II. Patient-specific geometries," *Physics of Fluids*, Vol. 31, No. 3, 2019, p. 031905. https://doi.org/10.1063/1.5081451.